Supporting Information:
Motion of 2D exciton in momentum space leads to pseudospin distribution narrowing on the Bloch Sphere

Garima Gupta[1], Kenji Watanabe[2], Takashi Taniguchi[3], and Kausik Majumdar[1,*]

[1]*Department of Electrical Communication Engineering, Indian Institute of Science, Bangalore 560012, India*

[2] *Research Center for Electronic and Optical Materials, National Institute for Materials Science, 1-1 Namiki, Tsukuba 305-0044, Japan*

[3] *Research Center for Materials Nanoarchitectonics, National Institute for Materials Science, 1-1 Namiki, Tsukuba 305-0044, Japan*

**Corresponding author, E-mail: kausikm@iisc.ac.in*

Note 1.

Dependence of exciton DOLP and DOCP on the exciton lifetime

The steady-state form of the time-dependent MSS equation (Eqn. 1 in the main manuscript) is given by:

$$\mathbf{G} = \frac{1}{\tau}\mathbf{S}(\mathbf{Q}) - \mathbf{\Omega}(\mathbf{Q}) \times \mathbf{S}(\mathbf{Q}) - \sum_{\mathbf{Q}'} \underbrace{\frac{w}{Q^2 \sin^2 \frac{\alpha}{2}}}_{\mathrm{W_{QQ'}}} [\mathbf{S}(\mathbf{Q}') - \mathbf{S}(\mathbf{Q})] \qquad (1)$$

The terms in the above equation are defined in the main manuscript. The momentum scattering rate expression $\mathrm{W_{QQ'}} = w/Q^2 \sin^2 \frac{\alpha}{2}$ (α represents the angle between the initial ($\mathbf{Q}$) and final ($\mathbf{Q}'$) state during scattering) corresponds to scattering of excitons with the charged impurities (see the supplementary information of ref. [1] for derivation). Using the above equation, we calculate the steady-state exciton DOLP (Fig S1.1) and DOCP (Fig. S1.2) as a function of momentum scattering rate scaling factor w, for different values of exciton lifetime τ. The exchange frequency remains constant in the calculation.

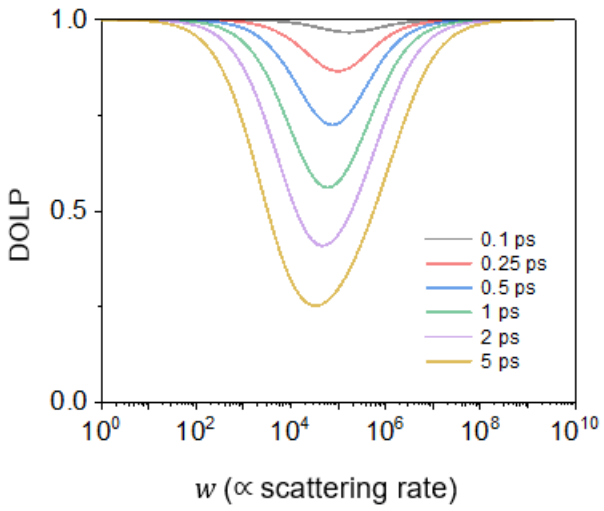

Fig. S1.1: Evolution of exciton DOLP as a function of momentum scattering rate at different exciton lifetimes (shown in the inset).

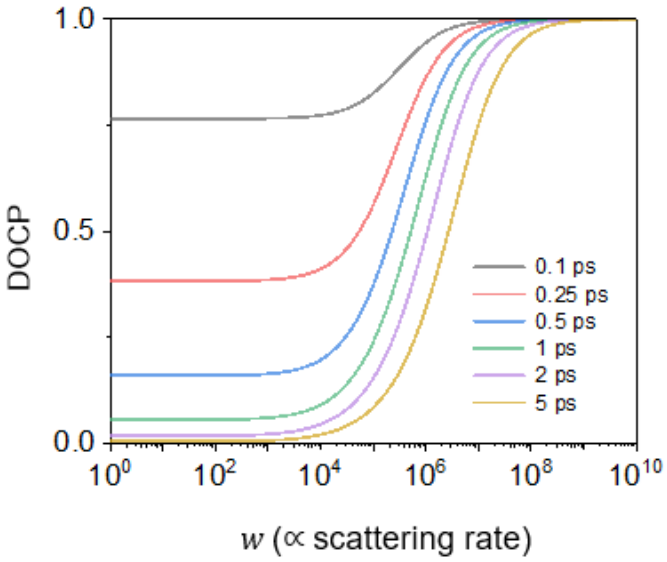

Fig. S1.2: Evolution of exciton DOCP as a function of momentum scattering rate at different exciton lifetimes (shown in the inset).

Thus, exciton valley polarization and valley coherence improve as the exciton lifetime reduces.

Note 2.

Calculation details of exciton DOLP and DOCP

The steady-state exciton DOLP ($\langle S_x \rangle$) or DOCP ($\langle S_z \rangle$) is obtained by solving for **S** using the following steady-state MSS vector equation[1]:

$$\mathbf{G} = -\mathbf{\Omega}(\mathbf{Q}) \times \mathbf{S}(\mathbf{Q}) + \frac{1}{\tau}\mathbf{S}(\mathbf{Q}) - \sum_{\mathbf{Q}'} \underbrace{\frac{w}{Q^2 \sin^2 \frac{\alpha}{2}}}_{\mathrm{W}_{\mathbf{QQ}'}} [\mathbf{S}(\mathbf{Q}') - \mathbf{S}(\mathbf{Q})]$$

$\mathbf{G}$ is the generate rate vector which is taken as either $[1,0,0]$ or $[0,0,1]$ depending on whether the excitation light is linearly or circularly polarized, respectively. The calculation of $\mathbf{\Omega}$ for the lowest energy $1s$ exciton, and the derivation of the expression for exciton-charged impurity momentum scattering rate $\mathrm{W}_{\mathbf{QQ}'} = w/Q^2 \sin^2 \frac{\alpha}{2}$ is taken from ref. [1]. α is the angle between the initial ($\mathbf{Q}$) and the final ($\mathbf{Q}'$) state during scattering. We vary the scaling factor w to obtain a varying exciton momentum scattering rate. The exciton lifetime has been taken to be $\tau = 3$ ps in our calculations[2–4].

Note 3.

Demonstrating DOCP ~ 0% in hBN-capped monolayer MoS_2

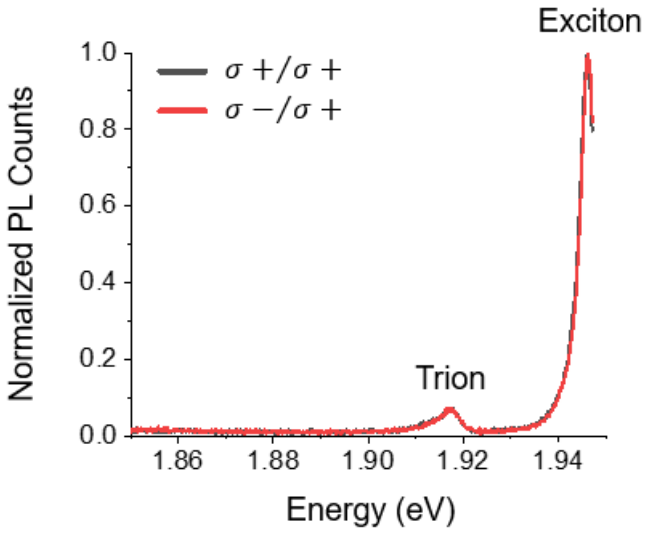

Fig. S3.1: Circular polarization resolved PL spectrum of a clean hBN-capped monolayer MoS_2 showing ~0% DOCP at 4 K. The fitted FWHM of the exciton peak is 4 meV. The excitation laser used is at 633 nm. The long-pass filter cuts off the higher energy part of the spectrum due to near-resonant excitation.

Note 4.

Monte Carlo Simulation Details

For the Monte Carlo simulation (Fig. 2 in the main manuscript), we generate 10^4 excitons at each $\mathbf{Q}$ state. We only generate excitons at $\mathbf{Q}$ states within the exciton light cone. For linearly polarized excitation, we generate excitons at $\phi = 0^0$ and 180^0 only, where ϕ is the polar angle in the exciton band in the momentum space. For circularly polarized excitation, the excitons are generated at all ϕ values. The steps in the Monte Carlo calculation of obtaining simultaneous exciton distribution in the momentum space and the Bloch sphere, as a function of time are as follows:

- **Calculation of free flight time and the exciton pseudospin precession between two scattering events**

An exciton at any state $\mathbf{Q}$ stays at the same state and undergoes scattering after a free flight time given by

$$t_f = -\frac{\ln r_1}{\mathrm{W}(\mathbf{Q})}$$

r_1 represents a random number with a uniform distribution between 0 and 1. $\mathrm{W}(\mathbf{Q})$ is the total momentum scattering rate at $\mathbf{Q}$ given by $\mathrm{W}(\mathbf{Q}) = \sum_{\mathbf{Q}'} \mathrm{W}_{\mathbf{Q}\mathbf{Q}'}$. During this time of flight, the exciton pseudospin undergoes presession about $\boldsymbol{\Omega}(\mathbf{Q})$. We obtain the modified S_x, S_y and S_z during the free flight time by using the cross product $\boldsymbol{\Omega}(\mathbf{Q}) \times \mathbf{S}(\mathbf{Q})$.

- **Selection of the new momentum state after scattering**

The final state after scattering is obtained by:

$$\Lambda_{\mathbf{Q},\mathbf{Q}'} < r_2 \leq \Lambda_{\mathbf{Q},\mathbf{Q}'+d\mathbf{Q}'}$$

r_2 is a another uniformly distributed random number between 0 and 1. $\Lambda_{\mathbf{Q}'}$ is defined as the successive summations from the first $\mathbf{Q_1}$ state till $\mathbf{Q}'$ normalized by the total scattering rate at $\mathbf{Q}$.

$$\Lambda_{\mathbf{Q},\mathbf{Q}'} = \frac{\sum_{\mathbf{Q_i}=\mathbf{Q_1}}^{\mathbf{Q}'} \mathrm{W}_{\mathbf{Q}\mathbf{Q_i}}}{\mathrm{W}(\mathbf{Q})}$$

- **Determination of the exciton lifetime**

The above two steps of free flight (and thus precession), followed by scattering are repeated till the lifetime of each exciton. The lifetime of the exciton is obtained by

$$t = -\tau \ln r_3$$

where r_3 is another uniformly distributed random number between 0 and 1. Here τ is the statistical exciton lifetime. We take $\tau = 3$ ps, typical exciton lifetime in monolayer TMDs.

Note 5.

Monte Carlo simulation results for exciton circular polarization

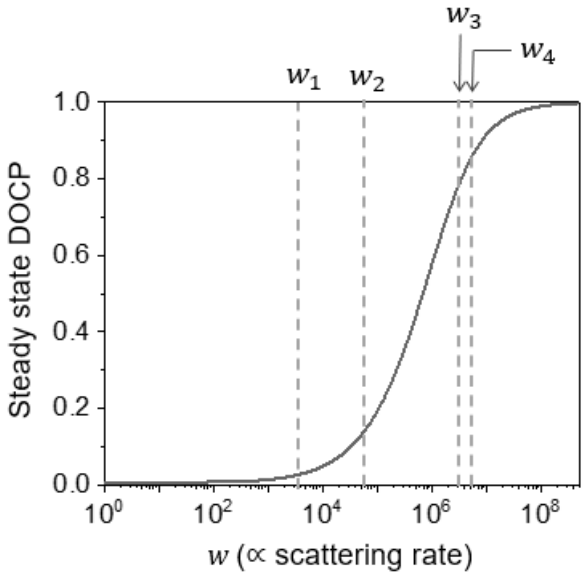

Fig. S5.1: Evolution of steady-state exciton DOCP as a function of momentum scattering rate. The four different values of momentum scattering rates (w_1, w_2, w_3, w_4) are chosen for further analysis.

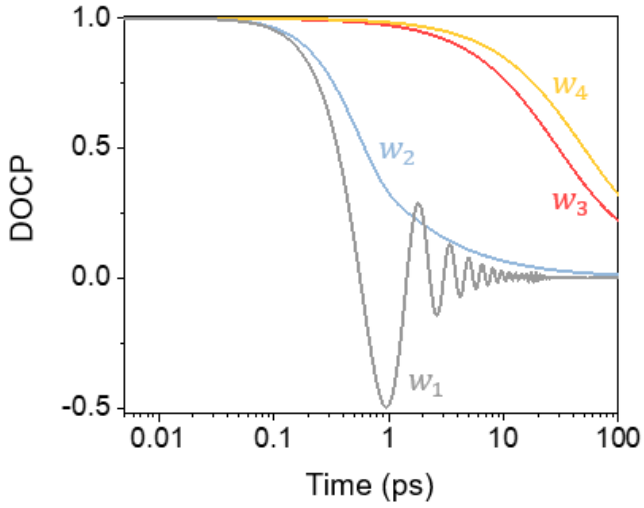

Fig. S5.2: Time-dependent evolution of exciton DOCP at the four different scattering rates highlighted in Fig. S5.1. Note that the oscillation at low scattering rates takes place due to pseudospin precession around **Ω** (see **Supporting video 1**). This happens when electron-hole spin exchange effect dominates over exciton momentum scattering.

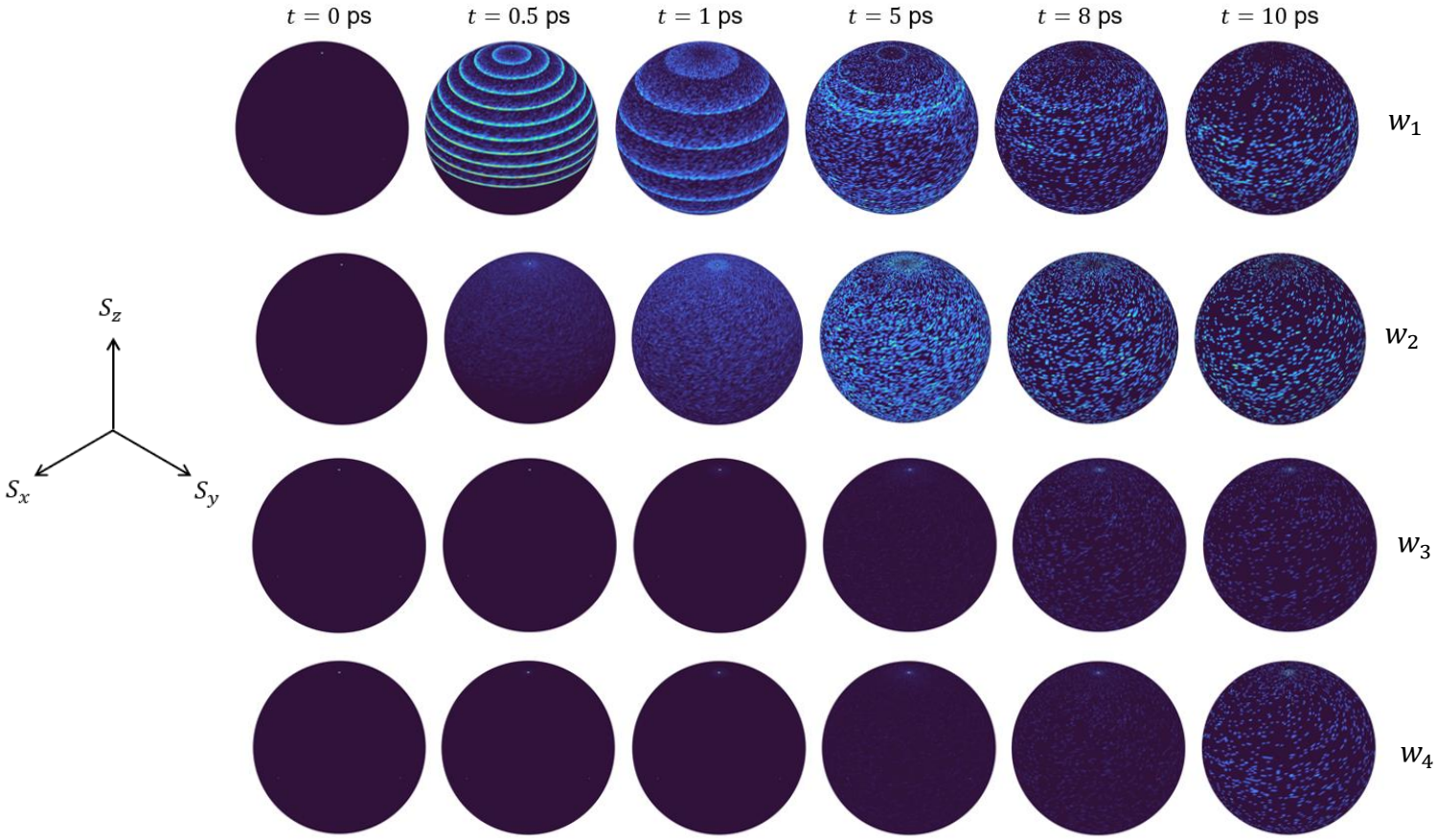

Fig. S5.3: Time evolution of the pseudospin phase distribution of the 10^4 circularly polarized generated excitons on the Bloch sphere obtained using the Monte Carlo simulation. The Bloch sphere axis orientation is shown on the left. The momentum scattering rate increases from the top row (w_1) to the bottom row (w_4). Note that the rings observed on the Bloch sphere at low scattering rate (w_1) appear due to the Q discretization in the calculation. Since Ω increases with Q, the different rings (corresponding to excitons residing at different Q states and precessing at different exchange frequency) appear. On the other hand, at large scattering rate (for example, w_3 and w_4), the narrowing of the pseudospin distribution around the north pole is evident, indicating motional narrowing effect for circular polarization.

Note 6.

Analytical derivation of the variance of the pseudospin distribution on the Bloch sphere in the motional narrowing regime

In between the $(i-1)$ and the i^{th} scattering event, an exciton at a state ϕ_i [$= \tan^{-1}(Q_{y,i}/Q_{x,i})$] in the **Q**-space, precesses about **Ω** oriented along $\hat{n}_i$ [$= \cos(2\phi_i)\ \hat{x} + \sin(2\phi_i)\ \hat{y}$]. Here Ω is the precession frequency. Before the next scattering event, the pseudospin rotates by an angle

$$\vec{\varphi}_i \ = \ \Omega\tau_i\hat{n}_i$$

on undergoing precession for scattering time τ_i. After many such scatterings, the pseudospin collects the rotation around various $\hat{n}_i$. Usually, rotations cannot be added vectorially as it does not commute with each other. However, this condition relaxes when the magnitude of rotation is infinitesimally small. In the scenario of commuting infinitesimal rotations, a vector addition of the rotations is possible.

In our scenario, the rotations are infinitesimal when $\Omega\tau_i \ll 1$, a condition that holds in the motional narrowing regime. Hence, the net rotation in the exciton pseudospin after *N* scattering events in the exciton lifetime is given by

$$\vec{\varphi} \ = \sum_{i=1}^{N} \vec{\varphi}_i = \sum_{i=1}^{N} \Omega\tau_i\hat{n}_i$$

For multiple such excitons, the variance in the magnitude φ $(= |\vec{\varphi}|)$ provides us the information about the extent of the pseudospin phase distribution on the Bloch Sphere, given as follows:

$$\sigma^2 \ = \ \langle\varphi^2\rangle - \langle\varphi\rangle^2$$

As $\langle\varphi\rangle^2$ goes to 0, the above equation becomes:

$$\sigma^2 \ = \ \langle\left(\sum_{i=1}^{N} \vec{\varphi}_i\right)^2\rangle$$

$$\sigma^2 \ = \sum_{i=1}^{N}\langle\varphi_i^2\rangle + \ 2\,\langle\sum_{i\,=\,1}^{N}\ \sum_{\substack{j\,=\,1 \\ j\neq i}}^{N} \vec{\varphi}_i.\vec{\varphi}_j\rangle$$

$$\sigma^2 \;=\; \Omega^2 \sum_{i=1}^{N} \langle \tau_i^2 \rangle + \; 2\Omega^2 \, \langle \sum_{i\,=\,1}^{N} \sum_{j\,=\,1, j\neq i}^{N} \tau_i \tau_j \, \hat{n}_i . \hat{n}_j \rangle$$

Since the lifetime τ_i and rotation axis $\hat{n}_i$ are independent of each other, the above equation is simplified as:

$$\sigma^2 \;=\; N\Omega^2 \langle \tau_i^2 \rangle + \; \Omega^2 N(N-1) \, \langle \tau_i \tau_j \rangle_{i \neq j} \, \langle \cos\big(2\phi_i - 2\phi_j\big) \rangle_{i \neq j}$$

We define $\langle \tau_i^2 \rangle = \tau_{rms}^2$, $\langle \tau_i \tau_j \rangle_{i \neq j} = \; \bar{\tau}^2$ (where $\bar{\tau} = \langle \tau_i \rangle$, since τ_i and τ_j are independent of each other), and $\langle \cos\big(2\phi_i - 2\phi_j\big) \rangle_{i \neq j} = f$.

$$\sigma^2(\varphi^2) \;=\; N\Omega^2 \tau_{rms}^2 \; + \; \Omega^2 N(N-1) \, \bar{\tau}^2 f$$

Approximating $\tau_{rms} \approx \; \bar{\tau} \approx \; \tau_s$ in the limit of very high scattering rate, we get

$$\sigma^2 \;\approx\; N^2 \Omega^2 \tau_s^2 \left(\frac{1}{N} \; + \; f \, \frac{[N-1]}{N} \right)$$

The term $N\tau_s$ can be approximated to be equal to exciton lifetime τ. Hence,

$$\sigma^2(\varphi^2) \;\approx\; \tau^2 \Omega^2 \left(\frac{1}{N} \; + \; f \, \frac{[N-1]}{N} \right)$$

Note 7.

Temperature dependence of exciton DOLP in monolayer MoS_2 on hBN

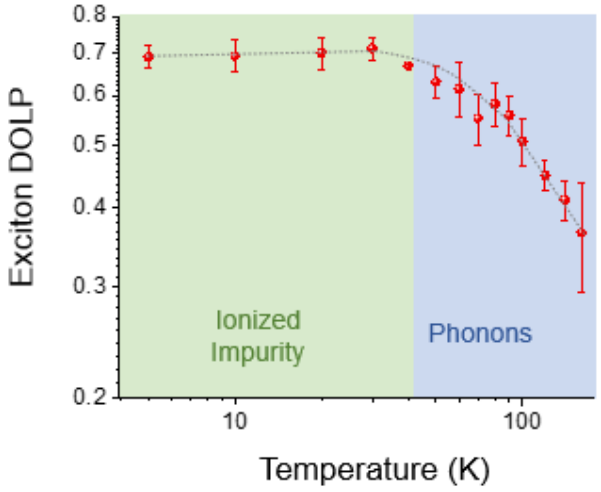

Fig. S7.1: Temperature dependence of exciton DOLP in monolayer MoS_2 on hBN. The green and the blue regions highlight the impurity scattering and phonon scattering dominated regions. The dashed black line is drawn as a guide to the eye.

Note 8.

Representative photoluminescence spectrum of hBN-capped monolayer MoS_2 showing weak trion peak intensity taken with 633 nm excitation

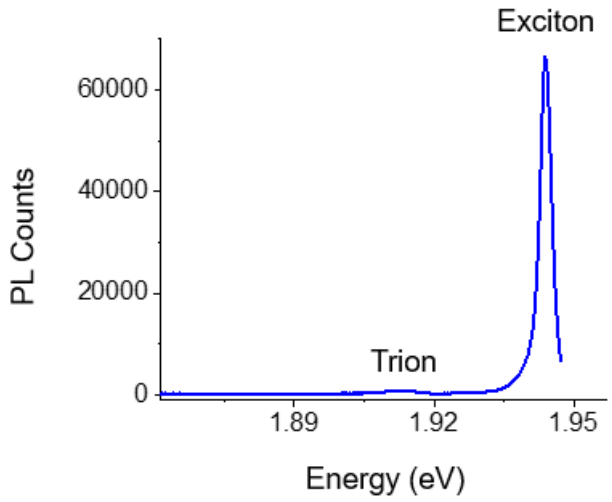

Fig. S8.1: A representative PL spectrum of monolayer MoS_2 capped with hBN on top and bottom showing weak trion peak as compared to the exciton peak at 4K (taken with 633 nm excitation laser). This implies that the exciton scattering with free carrier can be neglected in our samples at low temperature. The fitted FWHM of the exciton peak in this spectrum is 2.9 meV.

Note 9.

Trion/exciton versus defect/exciton ratio

Table S9.1 below compares the trion and defect intensity (normalized with the exciton intensity) in different stacks (stack A: monolayer MoS_2 sandwiched between two hBN flakes; stack B: monolayer MoS_2 on hBN)

	Trion/Exciton	Defect/Exciton	Defect/Trion
Stack A (Average taken over 39 points)	0.069	0.375	5.44
Stack B (Average taken over 10 points)	0.106	9.987	94.039
Stack B/Stack A	1.54	26.6	

Table S9.1: Comparison of average trion and defect peak intensity (both normalized with the exciton peak intensity) between stack A and stack B.

We can infer the following from the table above:

(a) The trion to exciton ratio in both the samples in much smaller as compared to the defect to exciton ratio. This implies that it is more probable for an exciton to scatter with an ionized impurity rather than a free electron (trion intensity directly reflecting electron density).

(b) When we go from stack A to stack B, the enhancement in the trion intensity (~1.54 times) is negligible as compared to the defect intensity (~26.6 times). This validates the main observation in this paper - a strong enhancement in the exciton DOLP (and DOCP) from stack A to stack B, due to motional narrowing induced by strong impurity scattering, which cannot be explained by free electron scattering as electron density remains similar in both the stacks.

Note 10.

System calibration data for polarization resolved measurement

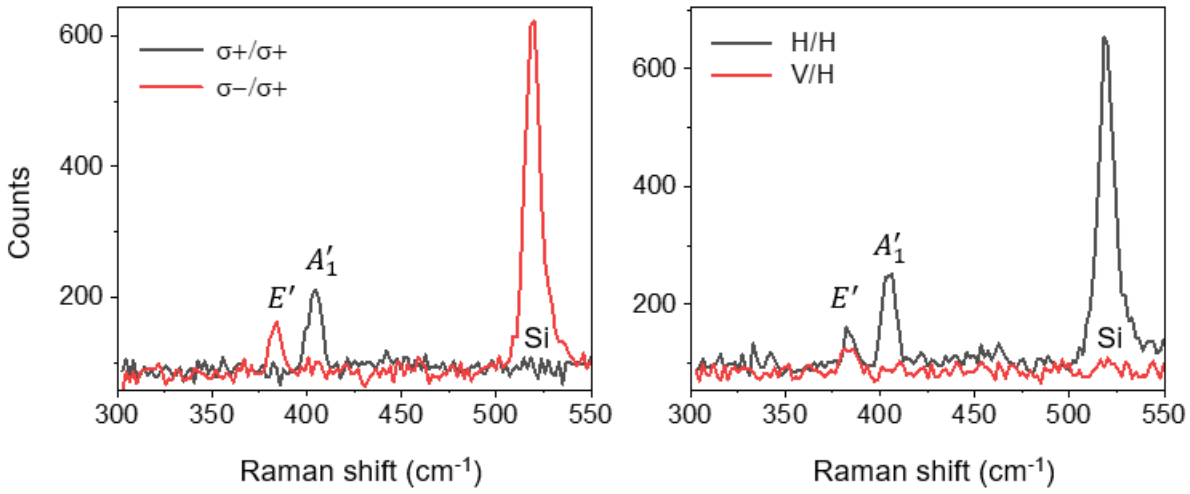

Fig. S10.1: Left panel: Circular polarization resolved Raman spectrum of monolayer MoS_2 showing an almost fully co-polarized MoS_2 A_1' Raman peak and a cross-polarized MoS_2 E' peak. The Si Raman peak is also fully cross-polarized[5]. **Right panel:** Linear polarization resolved Raman spectrum of monolayer MoS_2 showing an almost fully co-polarized MoS_2 A_1' Raman peak. Note that, MoS_2 E' Raman mode is not expected to be co-linearly polarized due to its Raman tensor[6]. The Si Raman peak is fully co-polarized. All the Raman spectra have been acquired at 295 K.

Note 11.

The fittings for Figs. 3c-f and 4b-c of main manuscript. For each spectrum, the top row shows the polarization resolved PL plots [in linear (left panel) and log (right panel) scale]. The bottom row shows the fitting of the corresponding co-polarized (left panel) and cross-polarized (right panel) spectrum in linear scale. The fitting is shown in a zoomed-in scale for better clarity.

Spectrum in Main manuscript Fig. 3c:

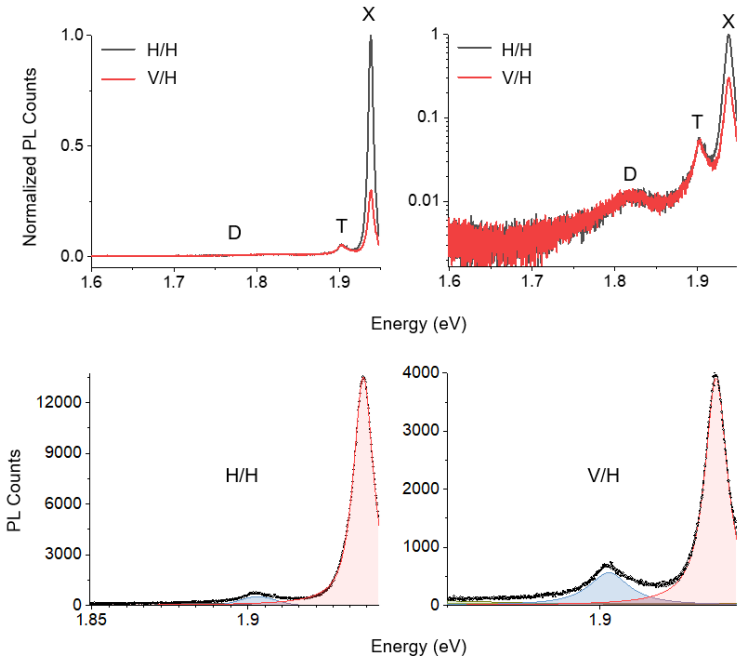

Spectrum in main manuscript Fig. 3d:

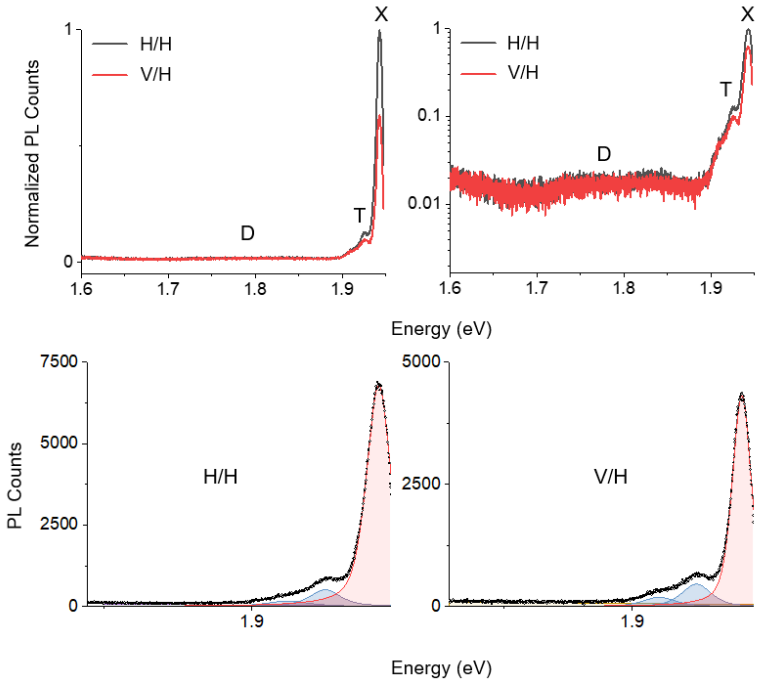

Spectrum in main manuscript Fig. 3e:

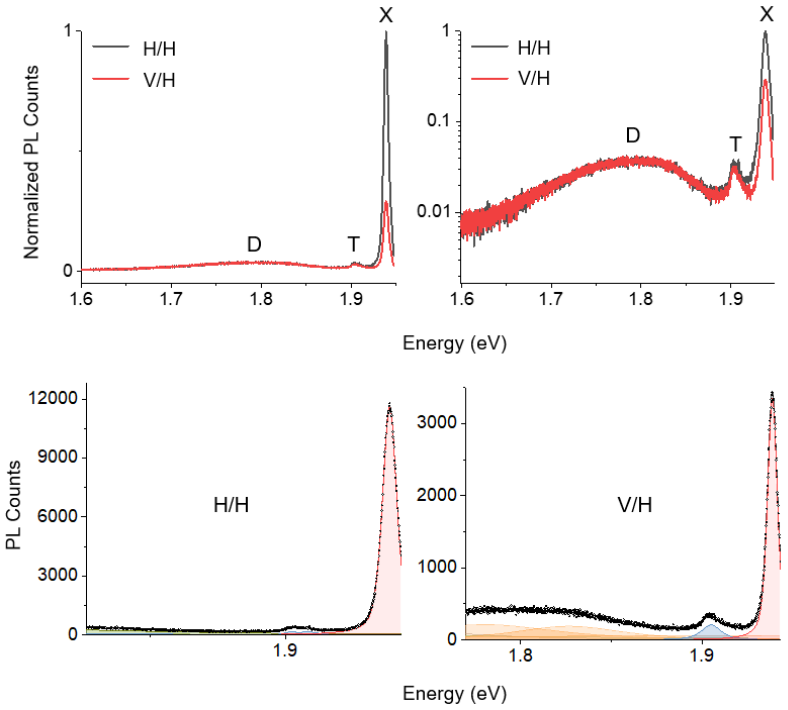

Spectrum in main manuscript Fig. 3f:

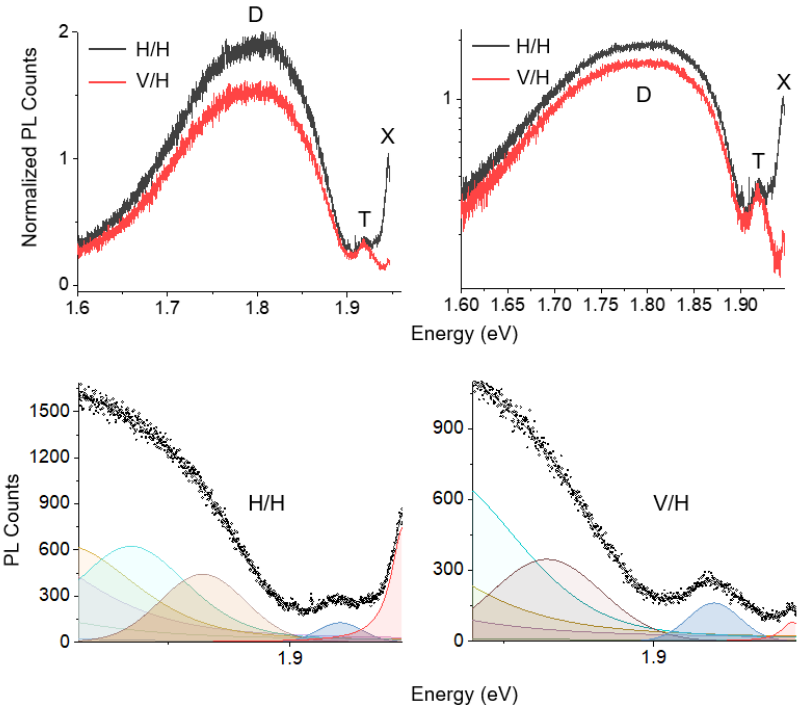

Spectrum in main manuscript Fig. 4b:

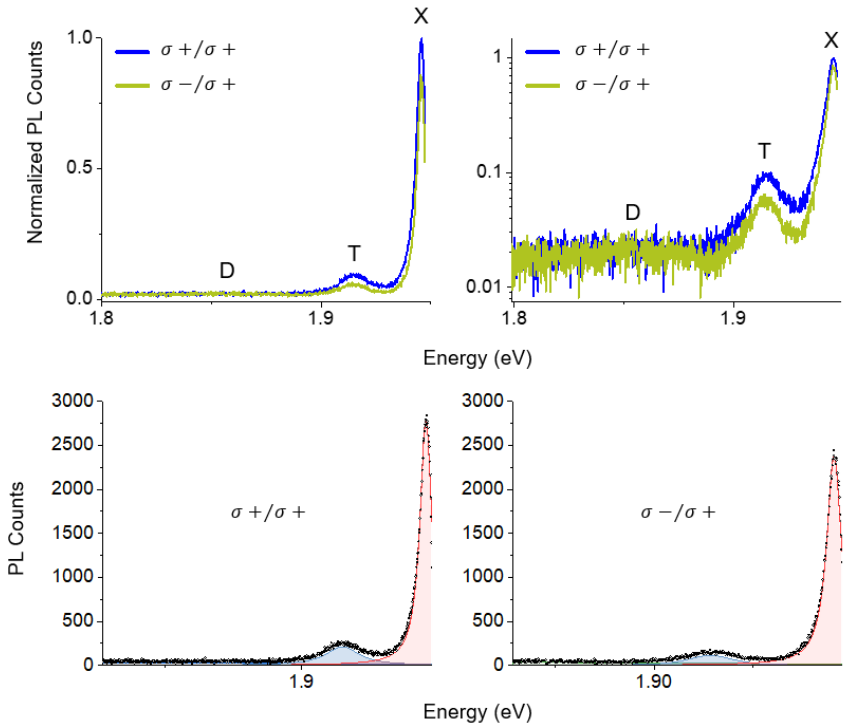

Spectrum in main manuscript Fig. 4c:

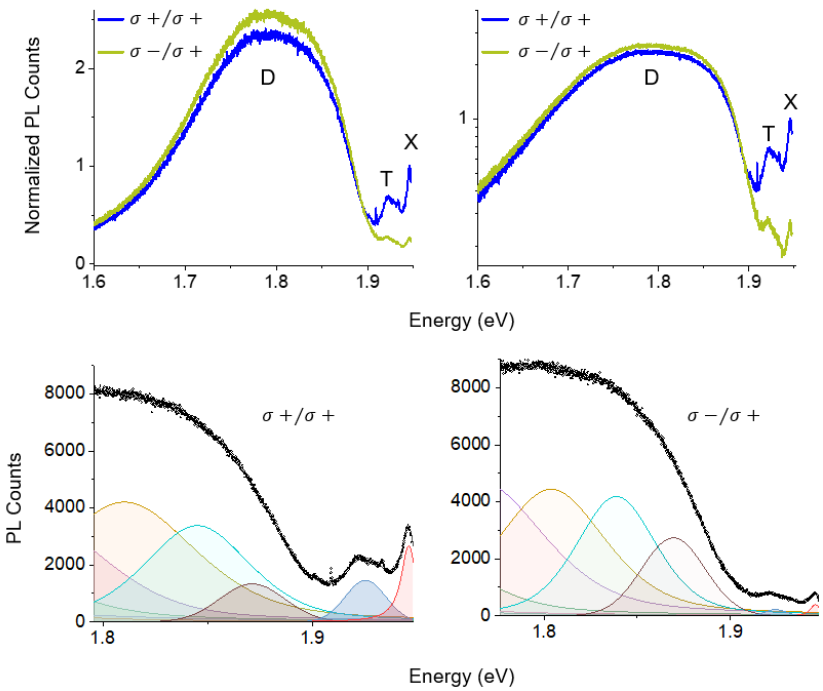

Note 12.

Polarization contrast as a function of momentum scattering rate at varying exciton lifetimes

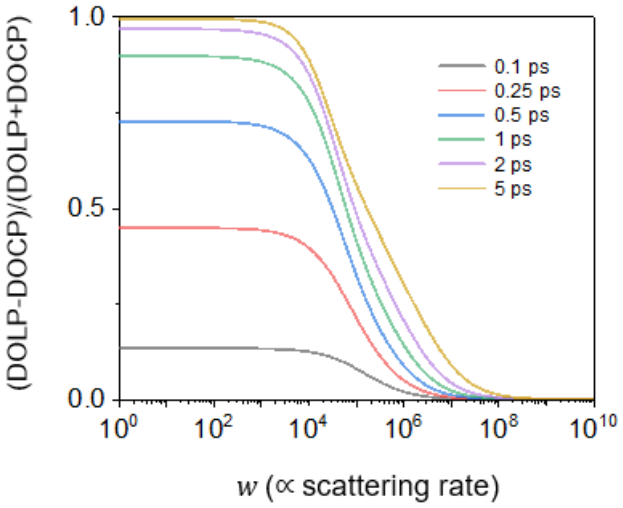

Fig. S12.1: Polarization contrast [PC = (DOLP-DOCP)/(DOCP+DOLP)] plotted as a function of momentum scattering rate at different exciton lifetimes.

References

1. Gupta, G., Watanabe, K., Taniguchi, T. & Majumdar, K. Observation of ~100% valley-coherent excitons in monolayer MoS2 through giant enhancement of valley coherence time. *Light Sci. Appl.* **12**, 173 (2023).

2. Palummo, M., Bernardi, M. & Grossman, J. C. Exciton radiative lifetimes in two-dimensional transition metal dichalcogenides. *Nano Lett.* **15**, 2794–2800 (2015).

3. Lorchat, E. *et al.* Filtering the photoluminescence spectra of atomically thin semiconductors with graphene. *Nat. Nanotechnol.* **15**, 283–288 (2020).

4. Robert, C. *et al.* Exciton radiative lifetime in transition metal dichalcogenide monolayers. *Phys. Rev. B* **93**, 205423 (2016).

5. Zhao, Y. *et al.* Characterization of Excitonic Nature in Raman Spectra Using Circularly Polarized Light. *ACS Nano* **14**, 10527–10535 (2020).

6. Chen, S. Y., Zheng, C., Fuhrer, M. S. & Yan, J. Helicity-Resolved Raman Scattering of MoS_2, $MoSe_2$, WS_2, and WSe_2 Atomic Layers. *Nano Lett.* **15**, 2526–2532 (2015).